https://doi.org/10.1051/e3sconf/202338204009

Soil-atmosphere interaction: cracking of a compacted soil under the effect of a thermo-hydric stress.

Sandrine Rosin-Paumier[1*], *Jaime* Granados[2], and *Bernardo* Caicedo[2]

[1] LEMTA - CNRS UMR 7563, Université de Lorraine, Nancy, France
[2] GeoSI – Department of Civil and Environmental Engineering, Universidad de Los Andes, Bogotá, Colombia

Abstract. Reusing excavated material in geotechnical engineering reduces the carbon impact of a project. Such materials are usually placed in a compacted state in order to achieve the mechanical and hydric characteristics required to guarantee the safety of the structures. A good geotechnical knowledge of the materials is therefore necessary as well as a good anticipation of their behaviour over time. Indeed, in some situations, as in the case of waste storage, a low hydraulic conductivity is required. The use of crushed rocks rich in clays (argillite), possibly improved by adding bentonite, could be interesting. However, this addition, beneficial in terms of hydraulic conductivity, could be damaging from a mechanical point of view by the development of cracks at the interface atmosphere-compacted soil. For this purpose, samples compacted at the normal Proctor optimum are exposed to a relative humidity of 46% and a temperature of 22.5°C. The thickness, mass and surface condition (cracking) were monitored during the drying process, and measurements were taken in the thickness of the specimen after 29 hours of exposure. The results make it possible to compare the two materials at the same compaction energy. The argillite sample shows a significant shrinkage but no cracks at this scale. On the different hand, with the addition of bentonite, a significant cracking was observed and analysed. These results provide information on the hydromechanical behaviour of unsaturated fine soils at the atmosphere-compacted soil interface.

1 Introduction

Reusing excavated materials in geotechnical engineering practice for underground backfill, construction of embankments or covering of landfills significantly reduces the carbon impact of a project. Indeed, this upcycling makes it possible to limit the extraction of natural materials (fewer careers) and to reduce transport distances and costs. Therefore, good understanding of the geotechnical interaction between excavated compacted soils and their environment is necessary to properly anticipate the soil behaviour over time.

Compaction is necessary to achieve the mechanical and hydraulic characteristics required to guarantee the safety and performance of geotechnical structures. In some situations, as in the case of waste storages, a low hydraulic conductivity is required [3]. The use of *in-situ* crushed rocks rich in clays (argillite), possibly improved by adding bentonite, could be interesting in these types of projects [8]. However, this addition, beneficial in terms of the initial hydraulic conductivity, could be damaging from a mechanical point of view due to the potential for cracks to develop at the interface between the compacted soil and the atmosphere. Li et al. [5] reported that, in the presence of desiccation cracks, the unsaturated hydraulic conductivity can increase by up to two orders of magnitude.

Soil desiccation cracking is a three-dimensional phenomenon that results from a complex interaction between the thermo-hydric stresses at the soil-atmosphere interface [10] and the suction that develops in the soil and generates tensile stresses that cause cracking [4]. Surface cracks can connect at various depths, forming networks that accelerate the drying of deeper layers [9, 11]. The presence of cracks decreases the erosion resistance, stability and bearing capacity of the soil, which in turn could compromise the stability and optimal functioning of the structures in service [1,2,6].

In this paper, compacted soil-atmosphere interactions for two thin clay materials were evaluated using a climatic chamber that simulates atmospheric conditions above the soil surface. A naturally excavated crushed clay and the same crushed clay added with MX80 bentonite were tested under controlled atmospheric conditions of air relative humidity (46%), air temperature (22.5°C), and air velocity ($1.0 m \cdot s^{-1}$). The samples were compacted near their maximum dry density and optimum water content based on the standard Proctor test. Initial sample dimensions were 0.24 x 0.24m² (area) by 18×10^{-3}m (thickness). The hydraulic properties of the samples were defined by means of the soil water retention curves. Thermo-hydric solicitations were imposed on the soil samples. Soil thickness, mass and surface condition (cracking) were monitored during drying. Finally, water content

* Corresponding author: sandrine.rosin@univ-lorraine.fr

https://doi.org/10.1051/e3sconf/202338204009

measurements were taken from the soil profile after 29 hours of solicitation (end of testing).

2 Methods

2.1 Determination of the soil water characteristic curves (SWCC).

Soil Water Characteristic Curves (SWCC) were obtained for two specimens of each soil (28.4×10^{-3} m diameter and 0.7×10^{-3} m thick) prepared near the normal Proctor optimum (OPN) densities and water content. Suctions were measured using a dewpoint potentiameter (WP4-T from Decagon Devices Inc.). The retention curves were determined from the wettest to the driest condition (drying path). Suction, mass and geometry of the soil samples were measured at several drying stages. Equilibration times of at least 24 hours between measurements were considered appropriate to achieve homogeneous soil water contents at each stage. During the equilibration time, samples were kept in sealed containers. SWCCs were calculated for both gravimetric and volumetric water contents.

2.2 Drying tests in a climatic chamber

A climatic chamber was used to evaluate the desiccation behaviour of two relatively thin compacted soil samples of naturally excavated crushed clay and a blend of crushed clay mixed with MX80 bentonite. The climatic chamber simulates steady atmospheric conditions of air relative humidity, temperature and wind velocity near the soil-atmosphere boundary (Fig.1). Air relative humidity and temperature are controlled with a set of heaters and *Peltier* plates and the wind is controlled with a centrifugal fan.

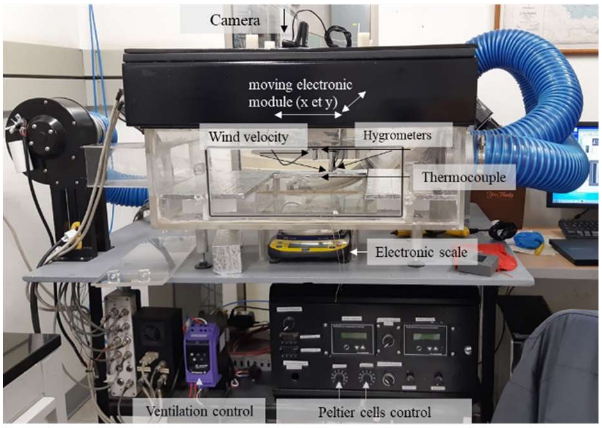

Fig. 1. General view of the climatic chamber.

Two air velocity sensors and two relative humidity sensors are installed on a moving electronic module at elevations of 5 and 25 $\times 10^{-3}$ m above the soil surface. The temperature of the air is measured with a set of thermocouples located at various positions along the airflow path. An infrared sensor is mounted on the moving electronic module to measure the temperature of the soil surface. Two thermocouples are placed within the soil. Details on the design and instrumentation of the climatic chamber may be found in previous publications (Lozada et al. 2016)[7].

After soil moisture conditioning and compaction, the samples were directly placed in the climatic chamber for the thermo-hydric solicitations. Average values of air temperature, relative humidity and wind velocity of 22.5°C, 46%, and 1.0 $m \cdot s^{-1}$, respectively, were selected for the tests presented in this study. An electronic scale recorded the water mass loss during soil desiccation. All electronic devices and sensors are connected to a data acquisition system that records during the tests at set intervals (10 seconds).

Finally, a digital camera was used to evaluate soil volumetric changes and cracking through image analysis. The images acquired throughout the tests were processed using the Image J software. The images, whose brightnesses have been adjusted, are binarised and then thresholded (Max Entropy). In this method, the area of the black pixels identified as background noise in the first image is subtracted from each image in the series. Each image was trimmed for shrinkage, and the number of black and white pixels was used to calculate the cracked area.

3 Materials

The materials were chosen based on the results obtained by Middelhoff (2020). The argillite was studied alone (Material A), or in a mixture of 70% argillite and 30% bentonite (Material A-B mix). The main known properties of these materials are shown in Table 1. The compaction condition chosen was near the maximum dry density and optimum water content of the normal Proctor test for each material.

Table 1. Mechanical properties of the studied argillite A, and the mix A-B 70/30 according to Middelhoff (2020).

Material	A	A-B mix
Specific gravity, G_s	2.68	2.64
Density, $\rho_{d\ OPN}$ (Mg/m^3)	1.83	1.45
Water content, w_{OPN} (%)	16.6	29
Liquid Limit, LL (%)	37.3	112.5
Plastic Limit, PL (%)	24.9	34.7
10% - Passing ($\times 10^{-3}$ m)	0.01	0.008
60% - Passing ($\times 10^{-3}$ m)	0.8	0.8

4 Results

4.1 Retention curves for each material

Two specimens of each material were compacted to a water content and dry density close to the optimum Proctor Normal (OPN) (Tab. 2). The compaction methodology achieved densities equivalent to 93.5% of OPN for the argillite and 97.2% of OPN for the A-B mix.

Table 2. Characterisation of the samples before drying to define the water retention curves.

Sample	A 1	A 2	A-B mix 1	A-B mix 2
Density, ρ_h (Mg/m^3)	2.02	1.99	1.83	1.8
Density, ρ_d (Mg/m^3)	1.72	1.7	1.42	1.4
Thickness (10^{-3} m)	7.33	7.45	7.09	7.17
Diameter (10^{-3} m)	28.4	28.4	28.4	28.4
Water content (%)	16.89	16.89	28.7	28.7
Void ratio, e	0.56	0.58	0.89	0.92
Saturation degree (%)	81.45	78.56	86.5	83.82

The evolution of water content, density and degree of saturation at each drying stage can be established by measuring the evolution of the masses and geometries of each specimen. The evolution of the soil suction, as a function of the degree of saturation and the density, is represented for each sample in Figure 2.

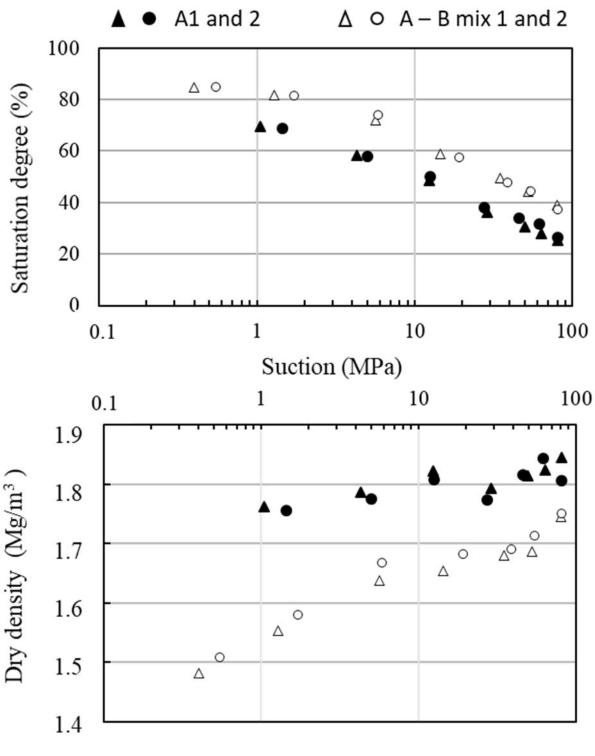

Fig. 2. Soil water characteristic curves (SWCC) along the drying path for the two samples A and A-B mix.

During the first drying stage, the suctions are relatively low and lower than the threshold of the potentiometer. Also during this initial drying, the shrinkage of the specimens offsets the water loss and the degree of saturation remains close to the initial value (above 80%). Subsequently, the shrinkage stabilises at dry density values near 1.82 Mg·m^{-3} for the argillite and 1.71 Mg·m^{-3} for the mixture. The shrinkage limit is reached at a water content of about 15% for the argillite and 18% for the mixture.

4.2 Drying test results

The following sections present the test results on the two soil samples exposed to similar dry environments (22°C and 46%) in the climatic chamber (Fig. 1). The mean air temperature, relative humidity and wind speed imposed on the soil surfaces and the corresponding variation ranges are given in Table 3, as well as the initial sample dimensions, water contents and dry densities. The water contents at the beginning of the test are 16.89% for A and 28.70% for the A-B mixture.

Table 3. Characteristics of the soil samples and atmospheric testing conditions in the environmental chamber.

Test	I	II
Material	A	A-B mix
Initial area (m x m)	0.24 x 0.24	0.24 x 0.24
Initial thickness (10^{-3} m)	18	18
Initial dry density (Mg/m^3)	1.83	1.45
Water content, $W_{initial}$ (%)	16.89	28.70
Wind velocity, V_{wind} (m/s)	1.01 +/- 0.13	1.02 +/- 0.08
Relative humidity, RH (%)	46 +/- 2	46 +/- 3
Air temperature, T (°C)	22.5 +/- 0.5	22.3+/- 0.6
Testing time (hours)	28.5	29.1

4.2.1 Shrinkage and cracking analyses

The evolution of the total surface area of the samples and water content during desiccation are shown over time in Figure 3. The initial area of both samples was 576 cm^2. However, a small part of the sample is not visible in the picture, the areas for image analyses were 527 cm^2 and 525 cm^2 for **Test I** and **Test II**, respectively.

It was observed that after 3 hours of conducting **Test I** (Argillite or Material A), the edges of the sample moved up a few millimetres while the centre remained at the same level forming a concave soil surface. This volumetric deformation affected the image analysis, as observed in Figure 3, where there are several scattered area datapoints. The soil movement increased the complexity of the image analysis during the first hours of testing. The movement also indicated that there were large strain-stress interactions at the soil-atmosphere boundary during the first hours of desiccation. To avoid contact between the moving electronic module that measures wind velocity, relative humidity, air temperature, and soil surface temperature, the module had to be positioned outside the limits of the sample for a few hours. For **Test II** (A-B mix), the evolution of the total surface area and the water content followed a comparable trend as observed for **Test I**.

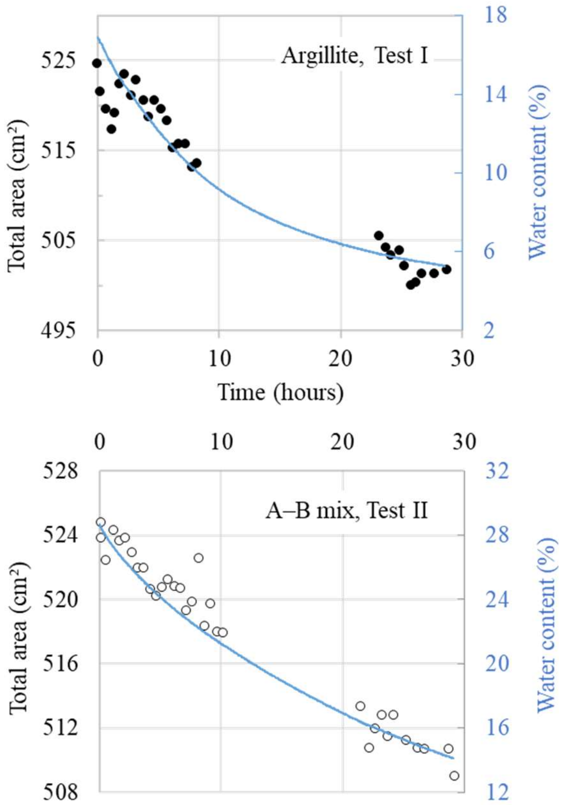

Fig. 3. Coupled evolution of the total area and the water content along time for tests I and II.

Regarding the evaporation rates observed in both tests, an initial intense evaporation phase took place during the first 4 to 6 hours of testing. During this time, the evaporation rates were approximately constant and the samples experienced significant shrinkage. Afterwards, this linear phase ends at approximately 6 to 8 hours of testing, and a less intense evaporation phase begins. This transition normally occurs between the Potential and Actual Evaporation phases. The lower evaporation rate can be explained by the fact that the drying crust that is formed at the soil-atmosphere interface prevents the water at the bottom of the sample from evaporating.

Regarding the cracking evolution, the overall observation of the series of images showed that the Argillite sample (**Test I**) remained uncracked throughout the test unlike the mix in **Test II**. For the A-B mix sample, many fine cracks appeared during the first hours of testing (see, for example Picture 8, Figure 4). Thus, the most accessible path for water to evaporate, after drying of the surficial layers, is the moist soil at the bottom of the cracks. The contact surface between air and moist soil is then small, and the evaporation rate slows down.

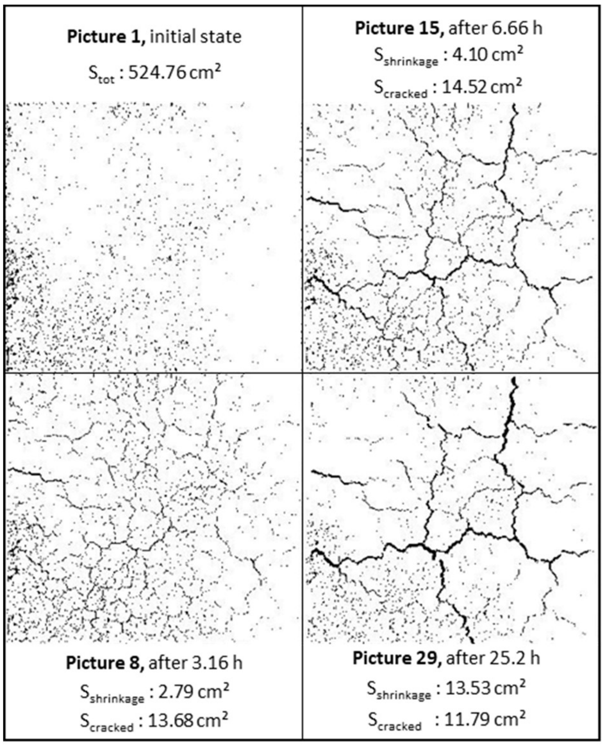

Fig. 4. Four examples of segmented pictures acquired during test II (A-B mix).

Under the effect of these internal forces, shrinkage continues, with some cracks developing in the majority to the detriment of others that are progressively refined and closed up. The network becomes less dense and more heterogeneous with time (see Pictures 15 and 29 in Figure 4). In each thresholded image, the cracks appear in black. The area of the black pixels in the first image is used to correct all the images in the series. Thus, the cracked area at a time t corresponds to the area of black pixels at time t minus the area of black pixels at initial state. In Figure 5, the evolution of the cracked surface and the shrinkage surface over time shows that the cracked surface reaches a maximum after about 4 hours. Thereafter, the cracked area decreases as the secondary cracks close in favour of the main cracks.

Throughout the test, the edges of the specimen are likely to lift under the intense action of the suction forces that develop during shrinkage. For the A-B mix sample, these deformations are visible but remain moderate. However, they could play a role in the selection of the main cracks since these cracks form geometric shapes at the end of the test (Picture 29, Figure 4). The evolution of the specimen depends on the hydric stresses, linked to evaporation, but also on the mechanical stresses, linked to the weight of the lifted parts. During the last hours of the test, the majority of the cracks extend through the sample. The broken specimen is once again flat and composed of several sub-units, each one evolving according to its own kinetics.

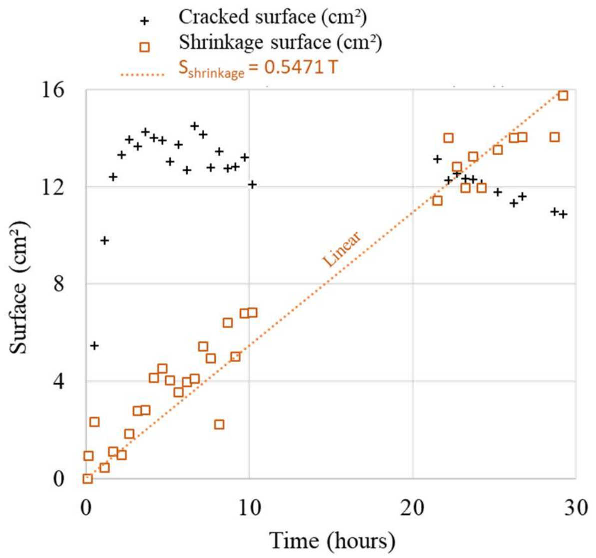

Fig. 5. Linear evolution of the shrinkage surface and cracked surface evolution during the test II.

4.2.2 Water content heterogeneity

Each sub-unit evolves according to the amount of water available in its centre. According to the measured mass of the specimen at the end of the test, the overall water content at the end of the test is 6.09% for Argillite (**Test I**) and 14.10% for A-B mix (**Test II**). However, the distribution of water changes with depth. Samples taken in successive layers through the thickness of the specimen made it possible to trace the water content profile within the specimen at the end of the test (Figure 6 and 7).

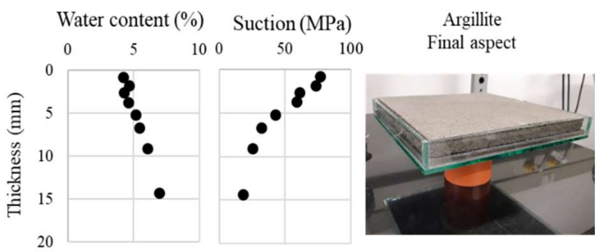

Fig. 6. Water content and suction measurements in the thickness of the Argillite sample at the end of the test I.

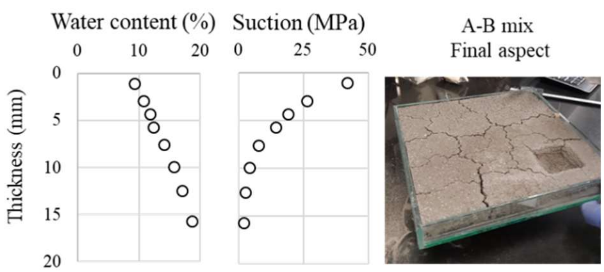

Fig. 7. Water content and suction measurements in the thickness of the A-B mix sample at the end of test II.

The initial moisture content of the A-B mix sample was 28.7% and its thickness was 18x10^{-3} m. At the end of the test, the bottom layers of the specimen retained more than 18% water content, while the surface layers contained less than 10% water content. The water content gradient with depth is almost linear for this material.

The thin-layer sampling method was also used to measure the evolution of suctions as a function of depth using the potentiameter. The measured values are consistent with the retention curves presented in Figure 2. The curves for the evolution of water content as a function of suction are shown in Figure 8.

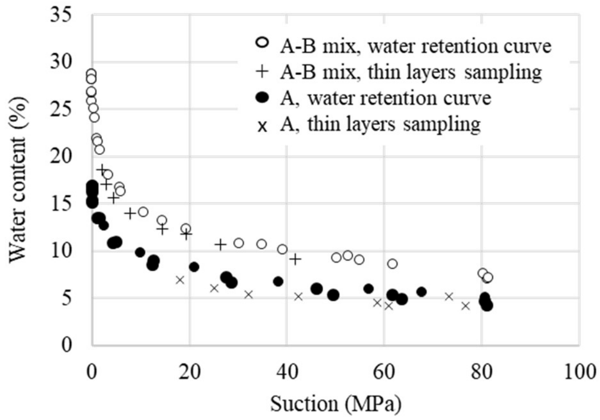

Fig. 8. Comparison of the water retention curves (A and A-B mix) and the suctions measured at the end of test I and II.

4.2.3 Temperature trends

Temperatures were measured at different locations. The results for **Test I** and **Test II** (A-B mix) are plotted in Figure 9a and 9b, respectively. For the A-B mix, the air temperature at the centre of the climatic chamber ($T_{Ambient}$) was relatively steady at 22.3°C (+/- 0.6°C). In contrast, the temperatures at the soil surface and within the soil (respectively named $T_{surface}$, T_1 and T_2), follow a complex evolution.

The temperature at the soil surface ($T_{surface}$) decreases significantly during the first hour of testing until it reaches a minimum temperature of 16.9°C. To 67 minutes of testing (1h07), i.e. a difference of 5.4°C compared to $T_{Ambient}$ was recorded. This is followed by a short period of stagnation at a temperature of 17°C until about 1.5 hours of testing. This difference can be explained by the heat exchanged during evaporation (latent heat of evaporation), consistent with the sharp decrease in water content during this period (see Figure 3). The soil temperature then rises significantly over the next 5.5 hours to 19.4°C, a deviation from the global air temperature of 2.9°C. This point coincides with the change in water evaporation rate (Figure 3) and the beginning of the decrease in the cracked surface (Figure 5). Over the next 23 hours, the soil temperature gradually increases until it reaches 20.4°C at the end of the test. The rate of diffusion of heat flow in the sample therefore appears to be an important factor in the cracking mechanism.

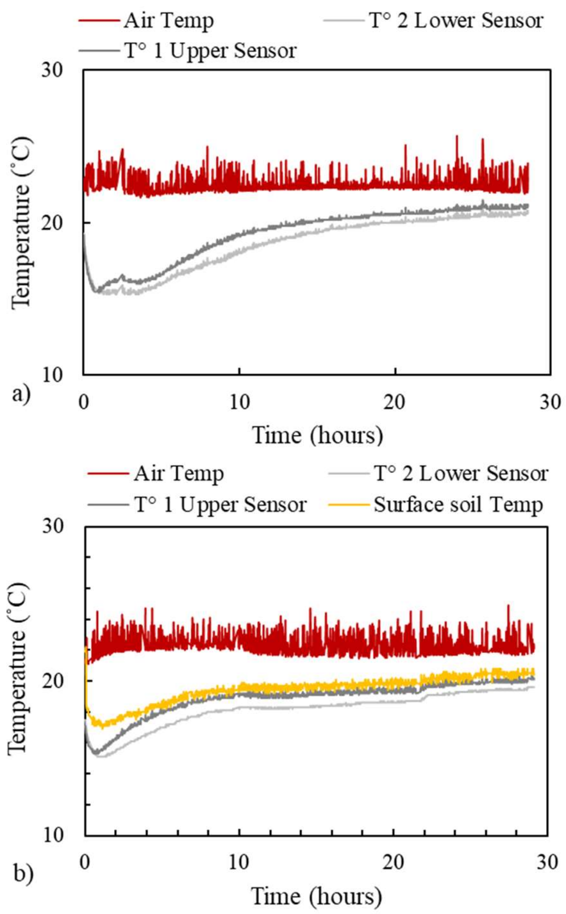

Fig. 9. Temperature evolution in different places of the samples a) A Test I, b) A-B mix, Test II.

5 Conclusions

In this study, two argillite soils compacted with the same compaction energy (normal Proctor) were subjected to controlled hydro-thermal solicitations. The two samples (0.24m side length) shrank significantly during desiccation. The shrinkage rate followed a similar pattern to that of the overall water content. Measurements of the water content profile at the end of the test made it possible to appreciate a water content gradient despite the small thickness of the sample. The drying front developed at the surface layers prevented to some extend evaporation from the lower layers.

Intense cracking of the sample containing 30% bentonite was measured. Its evolution was complex, passing through a maximum after 4 hours of testing. This evolution was probably linked to the solicitation of the lower layers of the sample via the cracks, which allowed the shrinkage of the whole soil mass and led to the selection of the main cracks.

This study also made it possible to monitor the temperatures within the samples. Temperature changes were consistent with the macroscopic phenomena. A decrease in temperature was observed during the first hours of testing, linked to the evaporation of pore water and heat of vaporization. When the quantity of accessible water for evaporation became more difficult to access due to the drying of the surface layers, the temperatures increased and reached a plateau, which is consistent with a lower rate of evaporation.

The results of this study will enable to better predict the conditions under which cracks appear in compacted soils and to develop control and remediation solutions.

Acknowledgments

This study is the result of an international collaboration made possible by the funding of scientific mobilities by the European project GEORES and by the NEEDS SolliScel project.

References

1. R. Auvray, S. Rosin-Paumier, A. Abdallah, F. Masrouri, EJECE **18** (1), pp.11 - 32.(2013)
2. Y.J. Cui, C.S. Tang, A.M. Tang, A.N. Ta, Rivista Italiana di Geotecnica, **24**, pp.9-20 (2014)
3. C. Gatabin, F. Plas, N. J. Michau, Tech. SFEN Feb, Paris, France (2016)
4. A. Ledesma, E3S Web of Conferences **9**, 03005 (2016)
5. J.H. Li, L. Li, R. Chen, D.Q. Li, Engineering Geology **206**, 33-41 (2016)
6. C. Lozada, B. Caicedo, L. Thorel, Géotechnique Letters **5**, 112–117 (2015)
7. Lozada, C, Caicedo, B, Thorel, L, 2016. E3S Web of Conferences **9**, 13002 (2016)
8. M. Middelhoff PhD thesis, Université de Lorraine, France (2020).
9. M.Sanchez, A. Atique, S. Kim, E. Romero, M. Zielinski, Acta Geotechnica **8**:583–596 (2013)
10. A. Ross, Stirling, Stephanie Glendinning, Colin T. Davie. Applied Clay Science **146**, 176-185 (2017)
11. C.S. Tang, C. Zhu, T. Leng, B. Shi, Q. Cheng, H. Zeng, Engineering Geology **255**, 1-10 (2019)